CrystEngComm

Cite this: *CrystEngComm*, 2012, **14**, 6264–6270

www.rsc.org/crystengcomm

PAPER

Concave Co_3O_4 octahedral mesocrystal: polymer-mediated synthesis and sensing properties

Yuanjun Liu,[a] Guoxing Zhu,[b] Baolong Ge,[a] Hu Zhou,[a] Aihua Yuan*[a] and Xiaoping Shen[b]

Received 9th February 2012, Accepted 11th June 2012
DOI: 10.1039/c2ce25788b

Co_3O_4 mesocrystals with concave octahedral structures were successfully prepared by a facile, polymer-mediated route. The Co_3O_4 mesocrystals are obtained from the oriented aggregation of primary nanocrystals from their six identical [100] directions. After a thorough investigation of their structure as a function of the adopted preparation parameters such as reaction time and the amount of polymer, the gas sensing performance of the Co_3O_4 mesocrystals was studied with formaldehyde and ethanol as probe analytes. It was found that they show high sensitivity and good response and recovery characteristics. As compared with Co_3O_4 powder, the Co_3O_4 mesocrystals exhibit 1.8-fold and 1.4-fold enhancement in gas responses to 100 ppm of formaldehyde and ethanol, respectively.

Introduction

Manipulating nanobuilding blocks into a highly ordered form has become an attractive topic in material design because it is one of the crucial steps to produce realistic nanodevices applied in various fields such as electronics, photonics, sensors, and catalysis.[1–3] Oriented aggregation (OA), observed by Melihov,[4,5] involves the self-assembly of primary nanocrystals, crystallographic reorganization within the self-assemblies, and transformation to oriented aggregates and has received increasing attention in recent years.[6,7] This non-classical crystallization pathway constitutes a facile strategy to fabricate complex superstructures. Compared with classical Ostwald ripening, OA growth provides a deeper understand of the micro/nano crystals growth. Cölfen and Niederberger have defined these oriented aggregates as mesocrystals.[8,9] Their distinct feature is that the primary nanocrystals in them are crystallographicaly oriented with single crystal-like atom structures and diffraction behaviors. The mesocrystals are constructed by subunit alignment, similar to highly sophisticated biominerals, and often have much higher porosities than conventional single crystals. They are promising substitutes for single-crystalline or porous polycrystalline materials in many applications such as catalysis, sensing, energy storage and conversion.

Since the concept of a mesocrystal was proposed, the number of known detected and established cases of mesocrystals has steadily increased, including not only biominerals and their mimetics[8,9] but also industrially important materials such as, WO_3,[10] TiO_2,[11,12] ZnO,[13,14] CuO_x,[15] V_2O_5[16] and so on. However, the spectrum of mesocrystals is still quite limited and the formation process is also poorly understood in many cases. Moreover, exploring the enhanced or new physical properties and chemical functions arising from the mesocrystalline superstructures of functional materials is demanding.

Co_3O_4, as one of most important p-type oxide semiconductors, has been widely studied owing to its applications in many fields, such as gas sensing, catalysis, and lithium-ion batteries.[17–20] So far, various micro-/nano-structured Co_3O_4 have been prepared, such as one-dimensional (1D) nanorod/wire/tube,[19,21,22] 2 D nanodisk/sheet,[23–27] 0 D nanocubes[28–30] and other sophisticated nanostructures.[31] But to the best of our knowledge, there are only a few reports about Co_3O_4 mesocrystal structures formed by the ordered self-assembly of primary nanocrystals.[32] Recently, Yao *et al.* reported the fabrication of single-crystalline Co_3O_4 hollow octahedral cages by a carbon-assisted carbonthermal method. Owing to the unique structure, they show improved lithium storage properties.[31]

Herein, we report for the first time the synthesis of concave Co_3O_4 octahedral mesocrystals through a polymer mediated solution phase process. The polyelectrolyte, poly (sodium 4-styrenesulfonate) (PSS), was used to modify the crystal growth process and is believed to play an effective role for the oriented aggregation of the primary Co_3O_4 nanocrystals by selective adsorption on some facets. The new nanoparticle-based Co_3O_4 octahedral mesocrystal is expected to have applications in gas sensing, catalysis, and lithium-ion batteries. After a thorough investigation of their structure as a function of the adopted preparation parameters, gas sensing performances were preliminary investigated in the detection of selected analytes (ethanol and formaldehyde), interesting for food quality monitoring and environmental proposes. Due to the unique microstructure, the obtained Co_3O_4 mesocrystals exhibit enhanced sensing performances than that of Co_3O_4 powder.

[a]*School of Biology and Chemical Engineering, Jiangsu University of Science and Technology, Zhenjiang, 212018, China. E-mail: aihuayuan@163.com; Fax: +86-511-85635850; Tel: +86-511-85638920*
[b]*School of Chemistry and Chemical Engineering, Jiangsu University, Zhenjiang, 212013, China*

Experimental section

Materials

Poly (sodium 4-styrenesulfonate) (PSS, M_w = 100 000 g mol^{-1}) aqueous solution (20 wt%, about 0.97 mmol g^{-1} based on the unit of $CH_2CHC_6H_4SO_3Na$) was purchased from Shanghai Herochem Corp., which is a slightly yellow solution but with relatively high viscosity. $Co(CH_3COO)_2{\cdot}2H_2O$ (A.R.) and Co_3O_4 powder were purchased from Sinopharm Chemical Reagent Co. Ltd. Deionized water was used throughout the experiment. All the chemicals were used without further purification.

Preparation of mesocrystal Co_3O_4

In a typical preparation process, 0.6 g of $Co(CH_3COO)_2{\cdot}2H_2O$ (2.7 mmol) and 3 g of poly(sodium 4-styrenesulfonate) (PSS, M_w = 100 000 g mol^{-1}) aqueous solution (containing 0.6 g of PSS, about 2.9 mmol based on the unit of $CH_2CHC_6H_4SO_3Na$) were orderly dissolved in 15 mL of distilled water with vigorous stirring for 30 min. The final mixture was transferred into a Teflon-lined chamber with a 20 mL of capacity, which was sealed and heated to 180 °C. After reaction for 24 h at this temperature, it was allowed to cool to room temperature naturally. The obtained black products were then collected by centrifugation and washed with deionized water and absolute ethanol for several times, and finally dried at 50 °C in vacuum for 12 h. For investigating the influence of experiment parameters on the microstructure, a serious of experiments was carried out with different reaction time (6 h, 12 h) or amount of PSS aqueous solution (1.8 g, 0.6 g, 0.2 g) but keeping other conditions constant.

Characterization

The crystal structure of the products were characterized by X-ray powder diffraction (XRD) (XRD-6000, Shimadzu Instrument, Japan) with Cu-Kα radiation (λ = 1.54060 Å) at a scanning rate of 4° min^{-1}. Scanning electron microscopy (SEM, Hitachi S-4800) was used to observe the morphologies and sizes. Transmission electron microscopy (TEM), high-resolution TEM (HRTEM) and the selected area electron diffraction (SAED) analysis were performed on a JEOL-2100 transmission electron microscope. The Fourier transform infrared spectra (FTIR) were recorded on a Nicolet Nexus 470 FTIR spectrophotometer using a KBr disk. The gas-sensing properties were measured on a WS-30A gas sensor measurement system (Weisheng Instruments Co., Zhengzhou, China) at a relative humidity of 20–35%.

Sensor fabrication and test

The gas sensor was fabricated similar to our previously reported ZnO sensor[33,34] and as follows: the typical Co_3O_4 samples were mixed with some terpineol binder to form a slurry through milling, and then pasted on to a ceramic tube to form a thin film between two Au electrodes, which were previously printed on the ceramic tube and were connected with four platinum wires.

A constant bias voltage was applied to the specimens. The working temperature of the sensor can be controlled by adjusting the heating voltage across a small Ni–Cr alloy coil located inside the ceramic tube. Scheme 1 shows a schematic drawing of a gas sensor. The gas sensors were aged for 8 h at working temperature (200 °C) before the test. The sensing response S is defined as R_g/R_a, where R_a is the sensor resistance in air and R_g is the sensor resistance in test gas.

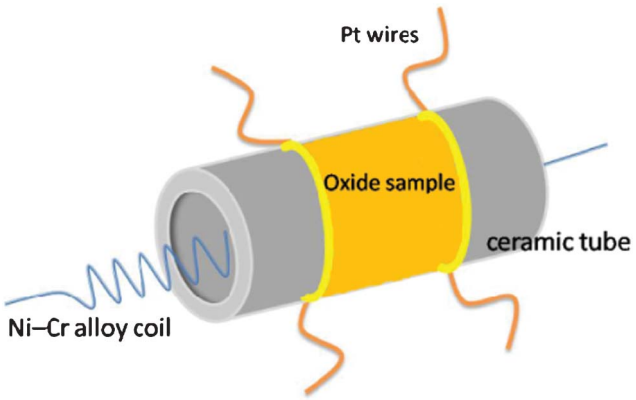

Scheme 1 Sketch of the gas sensor.

Results and discussion

Octahedral Co_3O_4 mesocrystals

The preparation of octahedral Co_3O_4 mesocrystals is through a polymer assisted hydrothermal route. The phase structure of the sample was firstly investigated by X-ray powder diffraction, the pattern of which can be easily indexed as that of cubic phase Co_3O_4 (Fig. 1, JCPDS No. 42–1467). The diffraction peaks are attributed to the (111), (220), (311), (222), (400), (422), (511), and (440) crystal planes of a cubic phase Co_3O_4. No characteristic peaks for impurities such as hydroxides are detected.

Fig. 2 shows the SEM images of the corresponding Co_3O_4 product, which show that the product is mainly composed of quasi-octahedron shape with a uniform size (Fig. 2a). The mean width (the length between two adjacent vertexes) is 430 nm, while the mean length is 560 nm. The SEM image with high-magnification shows that the obtained polyhedra have a well-defined shape with an uneven surface. The octahedral micro-crystal exhibits concave features in each tri-angle plane (Fig. 2b), which reveals that the polyhedron is in fact an icositetrahedron. This is quite different from the reported Co_3O_4 octahedral cages in that the surface is flat and smooth but with holes.[31] More interestingly, nanoparticles with clear interfaces are observed in/

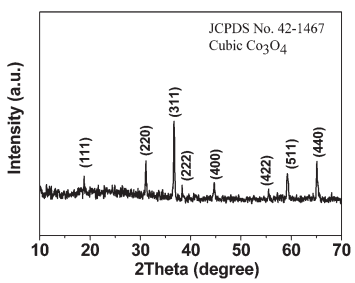

Fig. 1 XRD pattern of the prepared Co_3O_4 product prepared with 3 g of PSS aqueous solution and reaction time of 24 h.

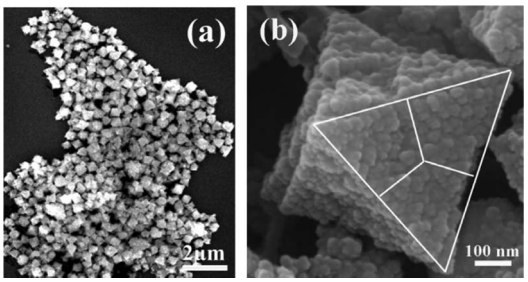

Fig. 2 (a) SEM image of the Co_3O_4 product prepared with 3 g of PSS aqueous solution and reaction time of 24 h. (b) An individual Co_3O_4 microcrystal showing the concave feature in its each tri-angle plane.

on the surface of the polyhedron, suggesting that they are assembled by these primary nanoparticles with a diameter of 20–50 nm.

The Co_3O_4 polyhedra were further characterized by TEM. Fig. 3a shows a typical low magnification TEM image of the as-prepared Co_3O_4 crystals. The Co_3O_4 polyhedra have different orientations on the surface of the carbon film for TEM observation and so show various cross-sectional shapes including a hexagram. Fig. 3b is a TEM image of an individual Co_3O_4 polyhedron with three vertexes supported on the carbon film. The fact that the octahedron is assembled by many tiny nanocrystals can also be clearly observed from the vertexes (Fig. 3b). More detailed crystal structural information of the polydron was provided by SAED patterns of the sixes vertexes shown in the insets of Fig. 3b. All insets show the single crystal-like diffraction spots with a [−111] axle, revealing the assembly of primary nanocrystals along the six identical [100] directions

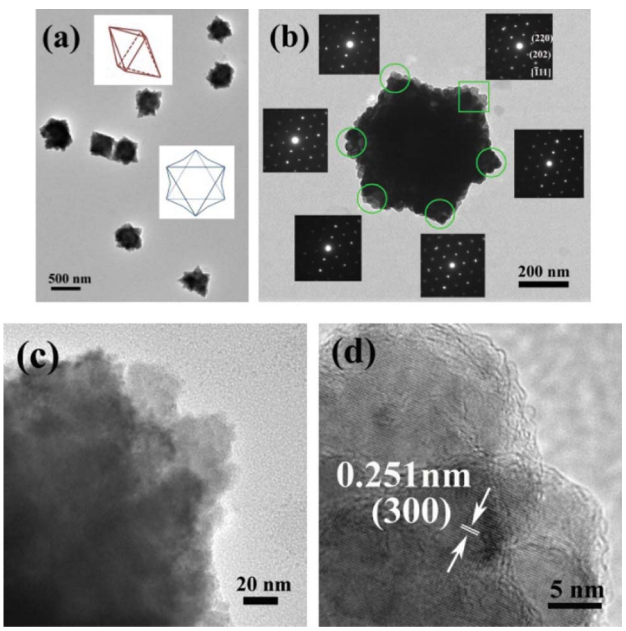

Fig. 3 (a) Low-magnification TEM image and (b) an individual particle of the Co_3O_4 octahedron prepared with 3 g of PSS aqueous solution and reaction time of 24 h. (c) and (d) The magnified TEM and HRTEM images of quadrate area of (b), respectively. Insets of (a) are schematic illustrations of the octahedron. Insets of (b) are the corresponding SAED pattern of each vertex.

forming six vertexes. The SAED pattern of the whole polyhedron particle also shows the same diffraction dot arrays, indicating that the individual nanocrystals within the icositetrahedron adopt the same crystal orientation. This further reveals the orientated attachment of the nanoparticle building blocks. The corresponding magnified TEM and HRTEM investigation of the square noted area of Fig. 3b are shown in Fig. 3c and 3d, from which the interfaces between different particles can be clearly seen. The observed lattice fringes with an interspacing of 0.251 nm can be indexed to the (300) plane of cubic plane Co_3O_4. All of these indicate that the obtained Co_3O_4 polyhedra are mesocrystalline in nature with six vertexes growing along the six identical [100] directions.

Fig. 4 shows the FTIR spectra of octahedral Co_3O_4 mesocrystals and PSS aqueous solution. The IR spectrum of the Co_3O_4 mesocrystal displays two distinct bands at 585 and 669 cm^{-1} originating from the stretching vibrations of the metal-oxygen bonds.[35,36] The first band at 585 cm^{-1} is associated with the OB_3 vibration, where B denotes Co^{3+} in the octahedral hole. The band at 669 cm^{-1} originates from the ABO_3 vibration, where A denotes Co^{2+} in the tetrahedral hole. Characteristic peaks at 1633 and 1009 cm^{-1}, attributable to stretching of C=C and the bending of C–H in the aromatic rings of PSS, are observed in both spectra. The peak at 1034 cm^{-1} assigned to the stretching vibrations of S=O is also observed in both. The peaks at 1190 and 1128 cm^{-1} (stretching vibrations of S–O)[37] in PSS have slightly shifted to 1159 and 1118 cm^{-1} for the Co_3O_4 sample, indicating the interaction of SO_3^- with the surface of the Co_3O_4 sample. These results suggest that the Co_3O_4 primary nanocrystals are covered with the PSS matrix.

For investigating the formation process of the concave Co_3O_4 octahedral mesocrystal, a controlled experiment with short reaction times was performed with other experimental parameters constant. Fig. 5a and b shows the TEM images of the product obtained after 6 h of reaction. The sample consists of many smaller nanoparticles in a size range of 3–8 nm. Some of them form larger agglomerates (Fig. 5a). The corresponding SAED pattern reveals a ring-like diffraction pattern, suggesting the different crystallographic orientation of these primary nanoparticles in the agglomerate. The HRTEM image shown in Fig. 5b demonstrating the irregular orientation between these primary nanoparticles further confirms this conclusion (Fig. 5b).

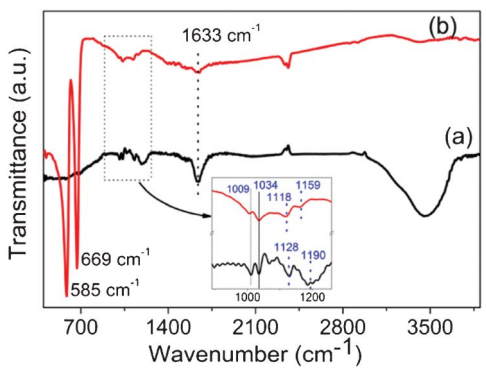

Fig. 4 FT-IR spectra of (a) PSS and (b) octahedral Co_3O_4 mesocrystals prepared with 3 g of PSS aqueous solution and reaction time of 24 h, the inset is the magnified spectra of the noted area.

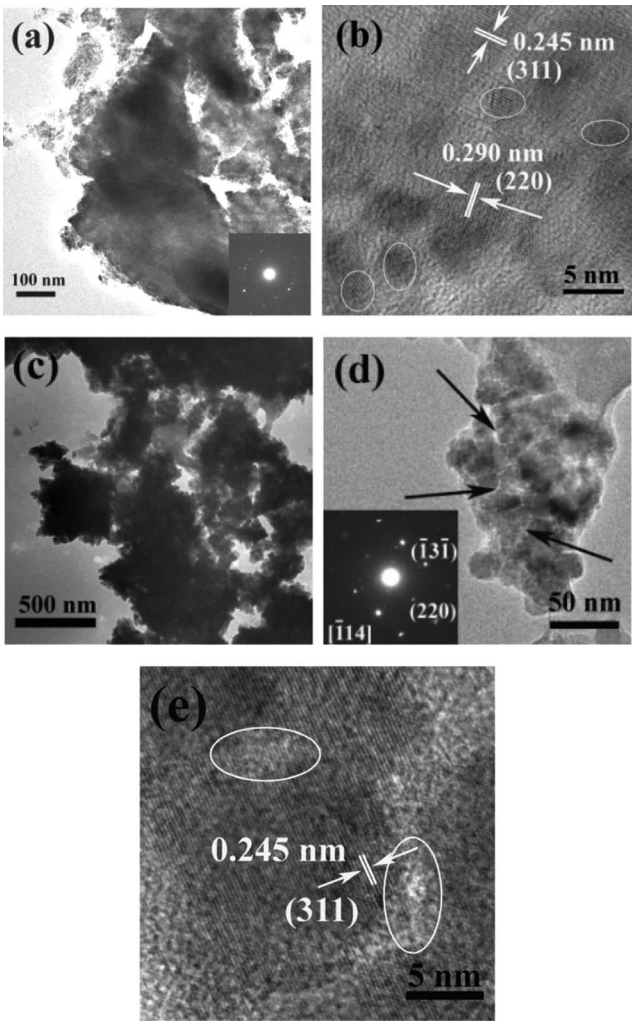

Fig. 5 TEM and HRTEM images of the Co_3O_4 nanostructure prepared with 3 g of PSS aqueous solution and reaction time of (a and b) 6 h and (c–e) 12 h. Insets of (a) and (d) are the corresponding SAED patterns. The circle mark in (b) shows the different orientation of the nanocrystals. The circles mark in (e) shows the void between neighboring building blocks.

The detected lattice fringes with an interspacing of 0.245 and 0.290 nm are in agreement with that of (311) and (220) facets of cubic phase Co_3O_4.

When the reaction time is lengthened to 12 h, as shown in Fig. 5c–e, the primary nanocrystals grow up into 20–30 nm and assemble into some agglomerates (Fig. 5c). The agglomeration of the primary nanocrystals is loose and leaving some small easily observed voids between neighboring building blocks within the whole structure (as shown by the arrows in Fig. 5d and the circles in Fig. 5e). The SAED pattern (inset of Fig. 5d) of the agglomerate exhibits a regular diffraction dot array like that of a single-crystal. These loose agglomerates give strong evidence to the growth of Co_3O_4 nanostructures following an oriented aggregation process, but not the classical crystallization route in which the crystal nuclei grow up *via* ion-by-ion addition and unit replication. The HRTEM analysis (Fig. 5e) shows continuous lattice fringes even across the spacing between the adjacent nanoparticles, which further confirms the identical crystallographic orientation among the primary nanocrystals. When the reaction time is up to 24 h, the octahedra were formed as shown in Fig. 2 and Fig. 3.

PSS plays an important role in the formation of Co_3O_4 mesocrystals. Fig. 6 shows the morphology of as-prepared Co_3O_4 nanostructures with different amounts of PSS aqueous solution (1.8 g, 0.6 g, 0.2 g) but the other experimental parameters kept constant (0.6 g of $Co(CH_3COO)_2{\cdot}2H_2O$ and reaction time of 24 h). It can be clearly seen that the yield of formed Co_3O_4 octahedral mesocrystals (the percentage of octahedron structures over all particles) will decrease as the amount of PSS decreases. Although about 80% of the octahedral mesocrystals are formed with 1.8 g of PSS aqueous solution, this value decreases to only about 10% when 0.6 g of PSS aqueous solution is used. Few octahedral Co_3O_4 mesocrystals are observed when 0.2 g of PSS aqueous solution is use and only some irregular structures are seen. Obviously, the PSS has a strong influence on the formation of Co_3O_4 mesocrystals. It is believed that the capping of PSS on the surface of primary Co_3O_4 nanocrystals plays a critical role for the oriented aggregation, although the influence from the reaction medium state induced by the addition of PSS with different amounts on the nucleation and growth of Co_3O_4 mesocrystals cannot be absolutely ruled out. In our case, the added PSS amount is lower. Considering the total volume of the reaction solution, the concentration of PSS is in the range of 0.032–0.002 g ml^{-1}, and the reaction systems have a similar state (viscosity) at room temperature for all the compared experiments. In addition, the reaction was carried out at a temperature of 180 °C, at which the state of the reaction medium would have little influence on the ion diffusion, local supersaturation, and particle nucleation.

Formation mechanism

Based on the above analysis, a possible formation mechanism of the octahedron mesocrystal is proposed. When the reaction temperature is increased to a certain value, the hydrolyzation of CH_3COO^- proceeds and causes the generation of OH^-, which would further react with Co^{2+} forming Co_3O_4 primary nanocrystals (Fig. 5b). At the same time, the PSS anions with negatively charged sulfonic acid groups in the side chain would anchor with cobalt sites on the surface of the Co_3O_4 nanocrystals through a chelating interaction between the cobalt and oxygen of PSS. Thus, the primary Co_3O_4 nanocrystals are covered with PSS anions.

It is widely considered that the shape of a nanocrystal with a cubic phase is determined by the growth rate ratio of the [111] direction to the [001] direction.[38] When the growth rate ratio equals to 1.73, an octahedron is obtained. For a mesocrystal

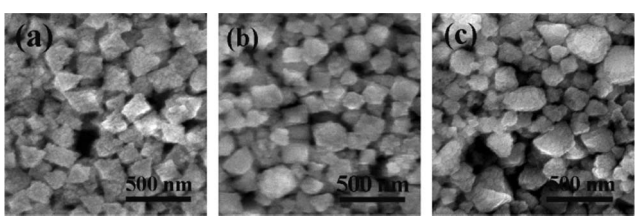

Fig. 6 SEM images of the as-prepared Co_3O_4 products with different amounts of PSS aqueous solution (a) 1.8 g, (b) 0.6 g, (c) 0.2 g.

grown by oriented attachment, its morphology may also depend on the aggregating rate ratio from these two directions. The {001} crystal planes of Co_3O_4 nanocrystals are composed of layers of Co^{2+} and Co^{3+}–O^{2-} (Scheme 2a). Both of the terminated {001} planes are covered with PSS anions (Scheme 2b). The adsorption of the polymer leads to crystal growth by aggregation of the primary nanoparticles rather than by coarsening. The aggregation occurs preferentially from a certain direction to minimize the mutual interaction energy according to the self-similarity rule.[13] The polymer, PSS, bonded on the {001} crystal planes has benzene rings in its chain which may act as a matrix for the oriented crystallization of Co_3O_4 building units in our case. Between the benzene rings from different primary nanobuilding blocks, some interactions such as π–π stacking exist. This interaction may help the oriented attachment of the primary nanocrystals from the six identical [100] directions, and causing the formation of Co_3O_4 octahedron (Scheme 2d).

While along the [111] directions, because the {111} crystal planes of cubic Co_3O_4 are polar planes composed of layers of Co^{2+}–Co^{3+} and O^{2-} (Scheme 2a, c), only one side of them can be covered with PSS. Thus, the attachment of primary nanocrystals from eight identical [111] directions is partly inhibited because of the electrostatic repulsion between O^{2-} terminated {111} planes and cobalt terminated {111} planes with PSS bonding. It seems that the inhibition of attachment from these directions is stronger, and the attachment rate ratio from [111] directions to [001] directions is smaller than 1.73, thereby giving rise to a concave octahedron.

The observed oriented attachment of Co_3O_4 nanocrystals form the [100] directions is different from that usually observed cases, in which the dipolar interaction of nanocrystals from one direction is usually considered to be the driving force for oriented attachment forming mesocrystals.[13,39] For Co_3O_4, the polar planes are {111} planes, however, as above mentioned, the oriented attachment of primary Co_3O_4 nanocrystals is not from the [111] direction but the [100] direction. This would be related to the preferential bonding of PSS on the Co^{2+}–Co^{3+} terminated {111} planes. The adsorption of the negatively charged polymer on the surface will counterpoise the bipolar actions along these directions. Thus the oriented aggregation growth mediated by PSS is concluded for the formation of Co_3O_4 mesocrystals. This is in contrast to the reported Co_3O_4 cage, in that case, the used carbon microspheres offer a weak reductive environment and template to promote nuclei preferential growth in a solid state reaction, inducing the formation of a single-crystal Co_3O_4 cage.[31]

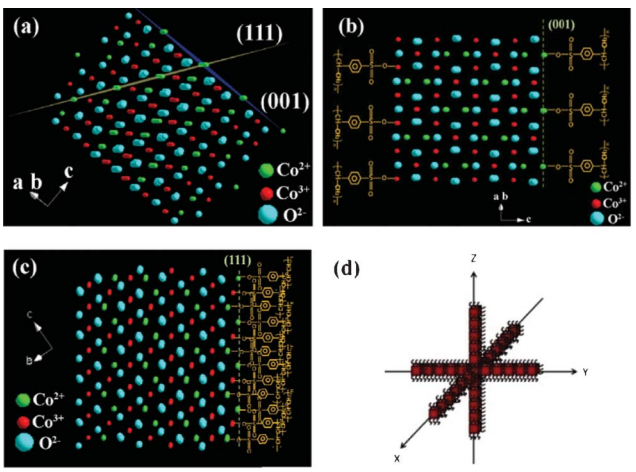

Scheme 2 (a) Co_3O_4 crystal structure and their (001), (111) planes. (b) The bonding of PSS on Co^{2+} or Co^{3+}–O^{2-} terminated (001) plane. (c) The bonding of PSS on Co^{2+}–Co^{3+} terminated (111) plane. (d) The schematic illustration of the growth of octahedral Co_3O_4 mesocrystal through the oriented attachment of Co_3O_4 nanocrystals.

Gas sensing

Co_3O_4 with conductivity highly sensitive to gaseous environments has been widely used as an effective, inexpensive gas sensing material for various toxic or pollutant gases/chemicals, such as ethanol, acetone, CO, NO_2, *etc.*[18,40,41] The prepared Co_3O_4 mesocrystal should show improved performance as a gas sensor since the voids between primary nanocrystals would provide a large surface-to-volume ratio and act as channels for the mass transportation of target gases, which is favorable for the sensing reactions of analyte gases. Here, the gas sensing properties of the Co_3O_4 mesocrystals were studied with formaldehyde and ethanol vapor as probe gases. Another sensor based on commercial Co_3O_4 powder was also fabricated for comparison.

Fig. 7a shows the representative dynamic gas response of the Co_3O_4 gas sensor to formaldehyde with concentrations ranging from 5 ppm to 1000 ppm. The resistances of the gas sensors increase when they are exposed to this reductive gas and recover to their initial state after exposing them to air, which is in agreement with that of a typical p-type semiconductor. The

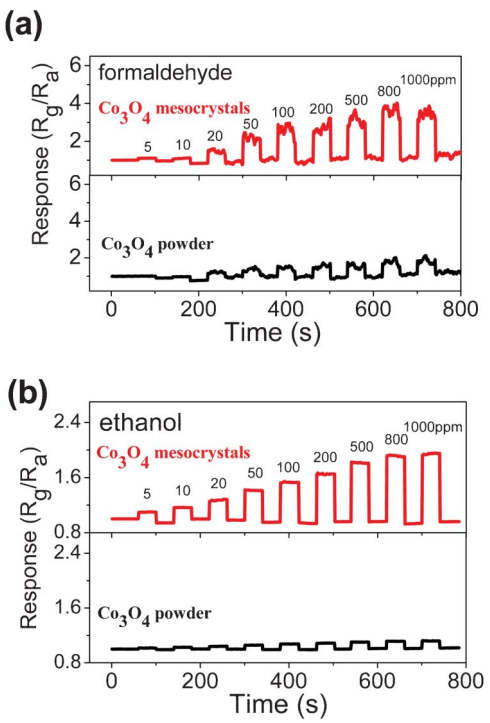

Fig. 7 The response-recovery curves of the two sensors based on the prepared Co_3O_4 mesocrystals and Co_3O_4 powder to (a) formaldehyde and (b) ethanol with different concentrations, respectively.

improved sensing performance of Co_3O_4 mesocrystals than that of commercial Co_3O_4 powder can be seen from the corresponding sensing response comparison of the two sensors. The sensing response of the Co_3O_4 mesocrystal sensor to 100 ppm of formaldehyde is around 2.8, in contrast to 1.5 with the Co_3O_4 powder. The sensing characteristics of the Co_3O_4 sensors to ethanol were also studied. As shown in Fig. 8b, the sensing characteristics are similar to that of formaldehyde. The sensing response of the Co_3O_4 mesocrystal sensor to 100 ppm of ethanol is around 1.5, which is also bigger than that of Co_3O_4 powder, 1.1. One also can see the good reversibility of the sensor, which is an important issue in the practical application.

The sensor responses as a function of gas concentrations are shown in Fig. 8a and 8b. For both tested gases, the sensing responses of the Co_3O_4 mesocrystal sensor increase with its vapor concentrations rapidly at first (below 100 ppm), while above that, the responses increase slowly and tend to saturation, indicating that the surface active sites are nearly fully covered with analyte molecules, or that the surface adsorbed oxygen species are not enough for the sensing reaction. While the sensing responses of the Co_3O_4 powder sensor only have a rapid increase with the concentration below 50 ppm.

The gas sensing mechanism for semiconducting metal oxides is widely ascribed to the change of electrical conductivity resulting from the chemical interaction of gas molecules with the surface of semiconductors,[33,42] which often involves gas adsorption, surface reaction, and desorption processes. In our case, when the Co_3O_4 sensor is exposed to air, oxygen molecules adsorb on the surface forming ionized oxygen species (O_2^-, O^{2-}, or O^-) [33,42] through trapping electrons from Co_3O_4 and causing an electron depleted layer on it. Thus, Co_3O_4 sensors show a highly conductive state in air due to the richness of holes, which are the main charge carriers for a p-type semiconductor such as Co_3O_4. When reductive gas molecules are introduced into the test chamber, they react with the oxygen species and release the trapped electrons. This effect eventually decreases the conductivity of the Co_3O_4 sensor. As a typical surface reaction, the sensor response greatly depends on the morphology, structure, size, and surface state of the sensing materials. The unique mesocrystal structure of Co_3O_4 induces the convenient gas diffusion and mass transportation in sensing materials. The many voids between primary nanocrystals would also provide more active sites for the sensing reactions. Thus, the Co_3O_4 mesocrystals show a higher sensing response.

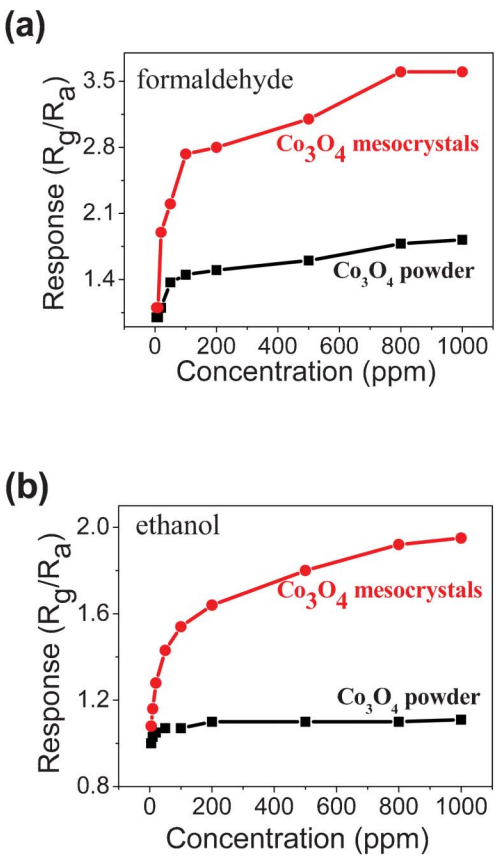

Fig. 8 The gas concentration-dependent responses of the two sensors to (a) formaldehyde and (b) ethanol, respectively.

Conclusions

In conclusion, concave Co_3O_4 octahedronal mesocrystals have been successfully synthesized through a polymer mediated route. The Co_3O_4 mesocrystals are formed by oriented aggregation of Co_3O_4 primary nanoparticles from their [100] directions. It is proposed that the anisotropic assembly is mediated through the different bonding of PSS on their crystal planes. The gas sensing properties of the Co_3O_4 mesocrystals were studied with formaldehyde and ethanol as probe gases. It was found that the Co_3O_4 mesocrystals display enhanced gas-sensing properties in comparison with Co_3O_4 powder. The strategy that uses a polyelectrolyte to modulate the surface properties and design the nanobuilding units would be a promising technique to fabricate functional mesocrystals and more complex nanostructures.

Acknowledgements

The authors are grateful for financial support from the Startup Fund for Distinguished Scholars (No. 35211103, 33211103), the National Natural Science Foundation of China (No. 51072071 and No.51102117), China Postdoctoral Science Foundation (2011M500085), Jiangsu Postdoctoral Science Foundation (1102001C).

References

1 C. P. Collier, R. J. Satkally, J. J. Shiang, S. E. Henrichs and J. R. Heath, *Science*, 1997, **277**, 1978–1981.
2 S. D. Sun, X. Z. Zhang, X. P. Song, S. H. Liang, L. Q. Wang and Z. M. Yang, *CrystEngComm*, 2012, **14**, 3545–3553.
3 M. P. Stoykovich and P. F. Nealey, *Mater. Today*, 2006, **9**, 20–29.
4 I. V. Melihov and A. S. Kelebeev, *Crystallography*, 1979, **24**, 410–412.
5 I. V. Melihov, I. V. Miheeva and V. N. Rudin, *Theore. Found. Chem. Techn.*, 1985, **19**, 742–748.
6 H. Cölfen and M. Antonietti, *Angew. Chem., Int. Ed.*, 2005, **44**, 5576–5591.
7 V. M. Yuwono, N. D. Burrows, J. A. Soltis and R. L. Penn, *J. Am. Chem. Soc.*, 2010, **132**, 2163–2165.
8 T. X. Wang, J. Mitchell, H. Börner, H. Cölfen and M. Antonietti, *Phys. Chem. Chem. Phys.*, 2010, **12**, 11984–11992.
9 M. Niederberger and H. Cölfen, *Phys. Chem. Chem. Phys.*, 2006, **8**, 3271–3287.
10 D. Wang, J. Li, X. Cao, G. S. Pang and S. H. Feng, *Chem. Commun.*, 2010, **46**, 7718–7720.

11 R. O. Da Silva, R. H. Goncalves, D. G. Stroppa, A. J. Ramirez and E. R. Leite, *Nanoscale*, 2011, **3**, 1910–1916.
12 J. F. Ye, W. Liu, J. G. Cai, S. Chen, X. W. Zhao, H. H. Zhou and L. M. Qi, *J. Am. Chem. Soc.*, 2011, **133**, 933–940.
13 Z. Liu, X. D. Wen, X. L. Wu, Y. J. Gao, H. T. Chen, J. Zhu and P. K. Chu, *J. Am. Chem. Soc.*, 2009, **131**, 9405–9412.
14 X. L.Wu, S. J. Xiong, Z. Liu, J. Chen, J. C. Shen, T. H. Li, P. H. Wu and P. K. Chu, *Nat. Nanotechnol.*, 2011, **6**, 103–106.
15 J. Romann, J. C. Valmalette, V. Chevallier and A. Merlen, *J. Phys. Chem. C*, 2010, **114**, 10677–10682.
16 C. Lausser, H. Cölfen and M. Antonietti, *ACS Nano*, 2011, **5**, 107–114.
17 W. Y. Li, L. N. Xu and J. Chen, *Adv. Funct. Mater.*, 2005, **15**, 851–857.
18 H. Nguyen and S. A. El-Safty, *J. Phys. Chem. C*, 2011, **115**, 8466–8474.
19 X. Xie, Y. Li, Z.Q. Liu, M. Haruta and W. Shen, *Nature*, 2009, **458**, 746–749.
20 X. W. Lou, D. Deng, J. Y. Lee, J. Feng and L. A. Archer, *Adv. Mater.*, 2008, **20**, 258–262.
21 X. W. Lou, D. Deng, J. Y. Lee and A. Archer, *J. Mater. Chem.*, 2008, **18**, 4397–4401.
22 Y. G. Li, B. Tan and Y. Y. Wu, *Nano Lett.*, 2008, **8**, 265–270.
23 J. Ryu, S.W. Kim, K. Kang and C. B. Park, *ACS Nano*, 2009, **4**, 159–164.
24 X. H. Liu, R. Yi, N. Zhang, R. R. Shi, X. G. Li and G. Z. Qiu, *Chem.–Asian J.*, 2008, **3**, 732–738.
25 Z. P. Liu, R. Z. Ma, M. Osada, K. Takada and T. Sasaki, *J. Am. Chem. Soc.*, 2005, **127**, 13869–13874.
26 J. T. Sampanthar and H. C. Zeng, *J. Am. Chem. Soc.*, 2002, **124**, 6668–6675.
27 M. Figlarz, J. Guenot and F. Fievetvincent, *J. Mater. Sci.*, 1976, **11**, 2267–2270.
28 J. Feng and H. C. Zeng, *Chem. Mater.*, 2003, **15**, 2829–2835.
29 X. H. Liu, G. Z. Qiu and X. G. Li, *Nanotechnology*, 2005, **16**, 3035–3040.
30 F. Cao, D. Q. Wang, R. P. Deng, J. K. Tang, S. Y. Song, Y. Q. Lei, S. Wang, S. Q. Su, X. G. Yang and H. J. Zhang, *CrystEngComm*, 2011, **13**, 2123–2129.
31 X. Wang, L. J. Yu, X. L. Wu, F. L. Yuan, Y. G. Guo, Y. Ma and J. N. Yao, *J. Phys. Chem. C*, 2009, **113**, 15553–15558.
32 T. He, D. R. Chen and X. L. Jiao, *Chem. Mater.*, 2004, **16**, 737–743.
33 G. X. Zhu, Y. J. Liu, H. Xu, Y. Chen, X. P. Shen and Z. Xu, *CrystEngComm*, 2012, **14**, 719–725.
34 G. X. Zhu, H. Xu, Y. J. Liu, Z. Y. Ji, X. P. Shen and Z. Xu, *Sens. Actuators, B*, 2012, **167**, 36–43.
35 C. W. Tang, C. B. Wang and S. H. Chien, *Thermochim. Acta*, 2008, **473**, 68–73.
36 C. Spenser and D. Schroeder, *Phys. Rev. B: Solid State*, 1974, **9**, 3658–3665.
37 X. H. Zhang, K. M. Ho, A. H. Wu, K. H. Wong and P. Li, *Langmuir*, 2010, **26**, 6009–6014.
38 S. E. Skrabalak and Y. N. Xia, *ACS Nano*, 2009, **3**, 10–15.
39 G. X. Zhu, S. G. Zhang, Z. Xu, J. Ma and X. P. Shen, *J. Am. Chem. Soc.*, 2011, **133**, 15605–15612.
40 M. Zhang and G. C. Jiang, *Chin. J. Chem. Phys.*, 2007, **20**, 315–318.
41 C. W. Na, H. S. Woo, I. D. Kim and J. H. Lee, *Chem. Commun.*, 2011, **47**, 5148–5150.
42 A. Gurlo and R. Riedal, *Angew. Chem., Int. Ed.*, 2007, **46**, 3826–3848.